TÜBİTAK

Turkish Journal of Earth Sciences

http://journals.tubitak.gov.tr/earth/

Research Article

Turkish J Earth Sci
(2023) 32: 632-651

doi:10.55730/1300-0985.1865

Evaluating the influence of recent tectonic activity on the river evolution using the identification of knickpoints in the south of Central Alborz Belt

Masoomeh ALAEI [1], Alireza NADIMI [1,*], Homayon SAFAEI [1], Maryam DEHBOZORGI [2]

[1]Department of Geology, University of Isfahan, Isfahan, Iran
[2]Department of Geology, Kharazmi University, Tehran, Iran

Received: 02.01.2023 • **Accepted/Published Online:** 09.05.2023 • **Final Version:** 28.07.2023

Abstract: Change in the steepness of river profiles caused by tectonic forces (uplift and material weakening in fault zones) causes the formation of the tectonically formed knickpoints (TFKs), which is an important geomorphic feature in bedrock river morphology. In this research, knickpoints in a wide area of the south of Central Alborz using the stream gradient (Gd) and the normalized steepness index (k_{sn}) were identified. According to the location of the knickpoints in relation to the faults in the area, the TFKs were identified. Analysis of the extracted TFKs with the longitudinal profile, logarithm slope-area plots, and natural logarithm gradient-distance plots confirmed their correspondence with the active segments of faults. Investigating the characteristics of TFKs such as length, height and gradient indicated that TFKs related to Mosha and North Tehran faults are high-altitude and the TFKs related to Taleghan and Eshtehard faults are long-distance. The identification of numerous TFKs on the active fault segments of the area and their confirmation based on field observations indicate a high rate of uplift and recent tectonic activity in the southern side of Central Alborz, which shows the importance of seismic studies due to the possibility of destructive earthquakes in the future.

Key words: Bedrock rivers, stream gradients, tectonically formed knickpoints, active tectonics, Central Alborz

1. Introduction

Several factors influence river networks; however, tectonics is one of the most important (e.g., Yildirim et al., 2011; Kirby and Whipple, 2012; Haghipour and Burg, 2014, Mandal et al., 2017; Peri et al., 2022; Kaveh-Firouz et al., 2023), as they are affected both by the ensuing mountain uplift (e.g., Whipple and Tucker, 1999; Bishop et al., 2005) and by material weakening in fault zones (e.g., Molnar et al., 2007; Koons et al., 2012). Therefore, the river sensitivity to climate and/or tectonic changes has made the quantitative analysis of channel morphology a valuable archive of active deformation (Schumm et al., 2000) in morphotectonic studies. Morphometric indices and longitudinal river profiles are used in landscape evolution and tectonic geomorphology studies (e.g., Merritts and Vincent, 1989; Snyder et al., 2000; Kirby and Whipple, 2012). Knickpoints are relatively steep reaches in longitudinal profile of a rivers, which are deviations from the characteristically smooth and concave form of both alluvial and bedrock rivers and usually considered as a response to the resistance of rock (Gardner, 1983; Miller, 1991) and tectonic activity (Bishop et al., 2005; Crosby and Whipple, 2006).

Factors influencing the creation of knickpoints can be referred to erosional resistance of bedrock (Miller, 1991), transient responses to base level fall (e.g., Castillo et al., 2013), tectonic activity (e.g., Bishop et al., 2005; Bull, 2007), and changes in load of sediment from tributaries (Jansen et al., 2011). A combination of the factor is often considered for the knickpoints origin (Phillips et al., 2010). Knickpoints are often known as the key to studying the geomorphological evolution of landscapes (Bishop et al., 2005; Hayakawa and Oguchi, 2009). In previous studies, knickzones were identified using visual control of longitudinal profiles, field observations and other data sources including topographic maps and high-resolution aerial photographs (e.g., Miller, 1991; Zaprowski et al., 2001; Duvall et al., 2004; Crosby and Whipple, 2006; Zhang et al., 2011). In such studies, often small numbers of knickzones were visually interpreted. Recent studies have provided a method to extract knickpoints in broad areas using digital elevation models (DEMs) and geographical information system (GIS) (Hayakawa and Oguchi, 2006, 2009), that can be used to extract river knickpoints in an area. In locating knickpoints which formed by tectonics

* Correspondence: a.nadimi@sci.ui.ac.ir,

(Kirby and Whipple, 2012; Lague, 2014; Boulton et al., 2014; Wei et al., 2015; Demoulin et al., 2017), it is very useful to use quantitative methods for precise evaluation of the relationship between recent tectonic activities and knickpoints in a vast area. In this study, using ASTER GDEM (30 m) in GIS and MATLAB software, changes in the river steepness (Whipple et al., 2007) in the southern flank of Central Alborz Belt were investigated. Also, after obtaining normalized steepness index (k_{sn}), the tectonically formed knickpoints (TFKs) were measured.

This area is affected by the NNE-SSW-trending contractional movements of the Arabian plate (e.g., Guest et al., 2006; Djamour et al., 2010; Rezaeian et al., 2012; Madanipour et al., 2013; Ballato et al., 2010, 2011, 2015) (Figure 1a) and there are many large and active faults in the area, which have been formed or reactive during the contractional movements. Moreover, comparison on the rate of vertical movement across the Central Alborz shows a progress of young deformation in Central Alborz toward the range southern hillside (Saberi et al., 2017). Therefore, this area is a suitable area for studying the characteristics of knickpoints and their relationship with the active segments of faults and river evolution. The purpose of this research is identifying TFKs and measuring their characteristics (length and height) and also identifying parts of active faults that have affected the slope of the river's longitudinal profiles in different parts of the southern Central Alborz Belt. The study of TFKs is useful and necessary for the evaluation of recent tectonic activities in the southern flank of Central Alborz Belt.

2. Regional setting

The study area (12,840 km^2) is located in the southern margin of Central Alborz Belt. The Alborz Belt in the north of Iran are part of the N-S-trending shortening between the Arabian and Eurasian plates. Present day N-S shortening and left-lateral shear across the Alborz Mountains occurs at 5 ± 2 mm/year and 4 ± 2 mm/year, respectively (Djamour et al., 2010; Vernant et al., 2004). Hence, the range has been deformed by strain partitioning of the oblique shortening in left-lateral strike-slip and thrust faults (Jackson et al., 2002; Allen et al., 2003). The studied area is affected by the northward movement of Central Iran in relation to Eurasia and also the southwestward movement of the South Caspian Block (Jackson et al., 2002; Ritz et al., 2006). The North Tehran, Taleghan, Firouzkuh and Mosha faults in the north and the Ipak and Eshtehard faults in the southwest are the main faults of the area (Berberian, 1983; Ritz et al., 2006; Nazari and Ritz, 2008; Nazari et al., 2009; Solaymani Azad et al., 2011; Ritz et al., 2012; Nazari et al., 2014) (Figure 1b).

Several historical earthquakes have been recorded in this area, the most notable is the one that destroyed almost 2000 villages in the area between Rey and Ivanki in 300 BC and destroyed Rey city completely. The magnitude of the earthquake was estimated about MS = 7.6 and IO = X (Ambraseys and Melville, 1982). The earthquakes of February 23, 958 AD in Rey-Taleghan, December 24, 1895 in Tehran, and May 1177 Rey-Qazvin occurred during the movement of the North Tehran Fault (Barberian et al., 1985; Nazari et al., 2010). The Malard earthquake on December 20, 2017 (Mw = 5.2) (https://www.usgs.gov) occurred at a depth of 12.8 km and about 30 km southwest of Tehran.

In the study area, a wide variety of sedimentary and volcanic rocks and unconsolidated sedimentary deposits, most of which range in age from Upper Precambrian through Quaternary have outcropped (Figure 1b). The oldest rock unit is the Upper Precambrian and Cambrian sedimentary rocks mainly consisting of sandstone, shale and limestone, which outcropped in the north of the study area. The Mesozoic sequence that includes dolomite, limestone, sandstone, shale, and conglomerate is widely observed in the area (Figure 1b). The Cenozoic sequence consists of shale, green tuff and volcanic rocks that are exposed especially in the northeast and southwest of the area. One of the most important sequences of Cenozoic is the Eocene volcanic and volcanoclastic complex of the Karaj Formation, with more than 3000 m thick (Figure 1b). The Plio-Quaternary deposits consist of conglomerate, sandstone, silt, sand, and clay (e.g., Rieben, 1955; Stöcklin, 1968; Alavi, 1996; Allen et al., 2003; Aghanabati, 2004; Zanchi et al., 2006; Guest et al., 2006; Ballato et al., 2008).

3. Data and methods

In this study, we used the 30-m ASTER global digital elevation model (GDEM) to extract the longitudinal river profiles in basins and finally, by examining the rivers steepness changes, the knickpoints in the area were identified.

3.1 River basin

Geomorphological analysis requires extraction of stream networks and river basins. To start the calculations, it is necessary to prepare the ASTER GDEM 30-m digital elevation model in Arc GIS 10.5 environment with using Arc Hydro program. First, to extract the drainage network in the study area, sinks of DEM were filled and the flow direction was extracted using the adjusted DEM values. Flow accumulation was created based on the flow direction and finally, the threshold with which the streams are defined was for the study area (12,840 km^2) based on the resolution of the DEM was determined. Morphometric parameters such as the number and order of stream were specified and according to the drainage flow density, rivers and drainage basins were extracted.

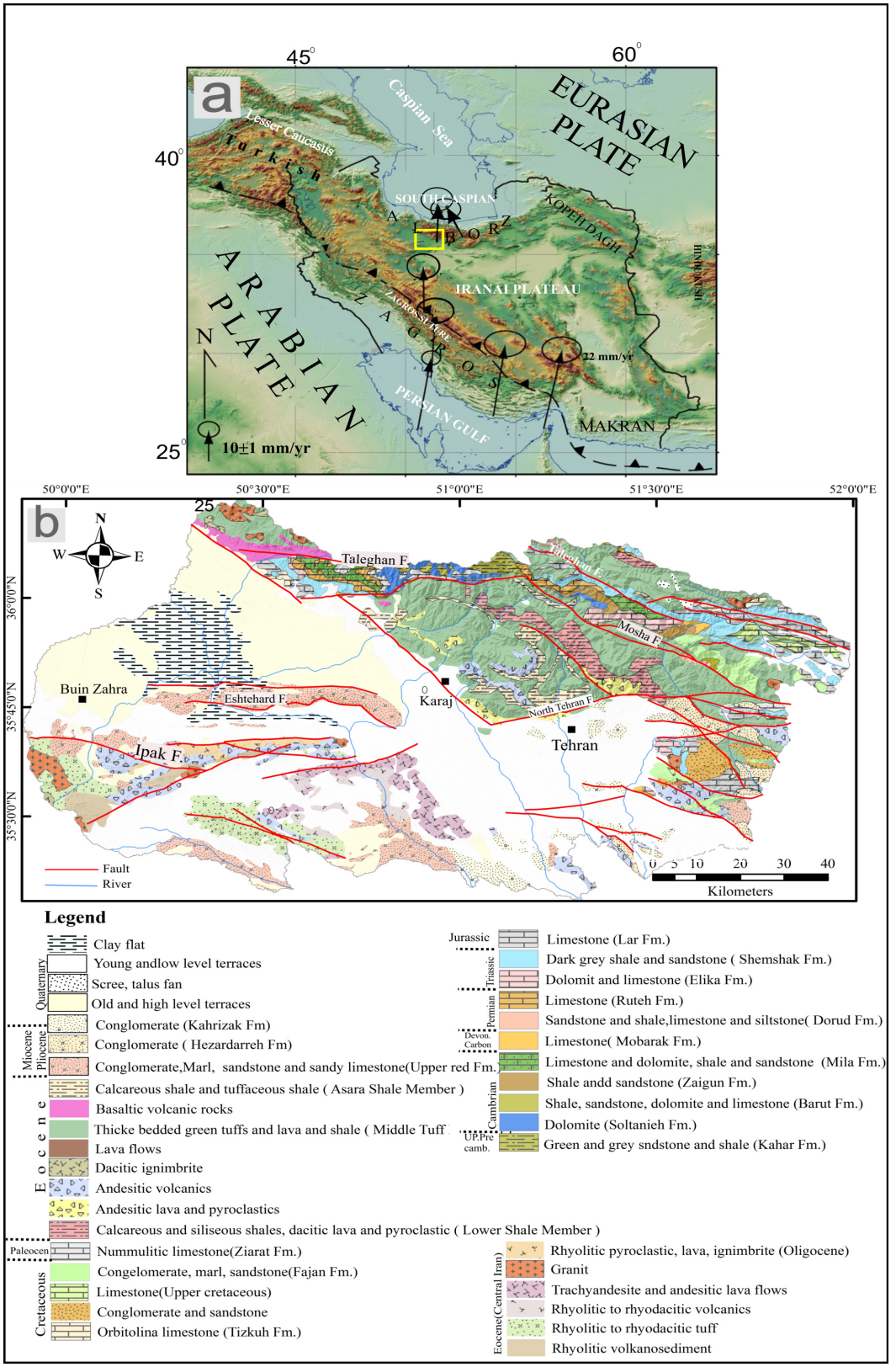

Figure 1. (a) Location of the study area and adjacent plates (modified after Guest et al., 2007). (b) Geological map of the study area (modified after Geological Map of Iran, 1:250,000 sheets Tehran, Saveh, Amol and Qazvin-Rasht).

The data verified with survey of topographical map (1:50,000) (published by National Geographical Organization, Iran) and the average planimetric error of the DEM, less than 20 m, and the vertical accuracy of DEM about 20 m was determined. The study area was divided into 23 sub-basins and their streams were drawn (Figure 2a).

3.2. The stream gradient (Gd)

The knickzone is a high-gradient part of the longitudinal profile of the river that is steeper than other parts. The knickpoint associated with a knickzone is located at the distinct inflection point between a knickzone and an upstream, lower gradient reach (Crosby and Whipple, 2006; Wobus et al., 2006). Most of the knickpoint are created in bedrock rivers. The analysis of knickpoint follows the methods described by Hayakawa and Oguchi (2006). At first, the stream gradient, Gd (m/m), is calculated at each point with a measurement length of d (m):

$$Gd = (e1 - e2)/d,$$

where d is the horizontal distance (m) which was used to calculation of gradient (m), and e1 and e2 are the riverbed elevations (m) at d/2 upstream and downstream of the measurement point, respectively (Hayakawa and Oguchi, 2006) that derived from the GDEM2 in GIS. According to the digital elevation model, which is 30 m, first the rivers were divided into points with a distance of 50 m, then the height of the points was obtained by using the GDEM2.

The measurement of Gd value is designed by MATLAB code at different points of the streamline. The length and height of points in strike a streamline, which is a vector file, is directly read by the MATLAB code.

Gd changes as a function of d, when d is small represents a local feature of river gradient, but it is a trend feature when d is large (Hayakawa and Oguchi, 2009), Gd also depends on the lithology of bedrock. In the region, the Gd index was calculated for each point for different values of d in all the rivers. The different values of Gd at each point for different d show that the Gd index is very variable for short distances (d < 1200 m) and shows a local river gradient and has little change in long distances (d < 1200) which is consistent with the results of previous studies (Figure 2b) (Hayakawa and

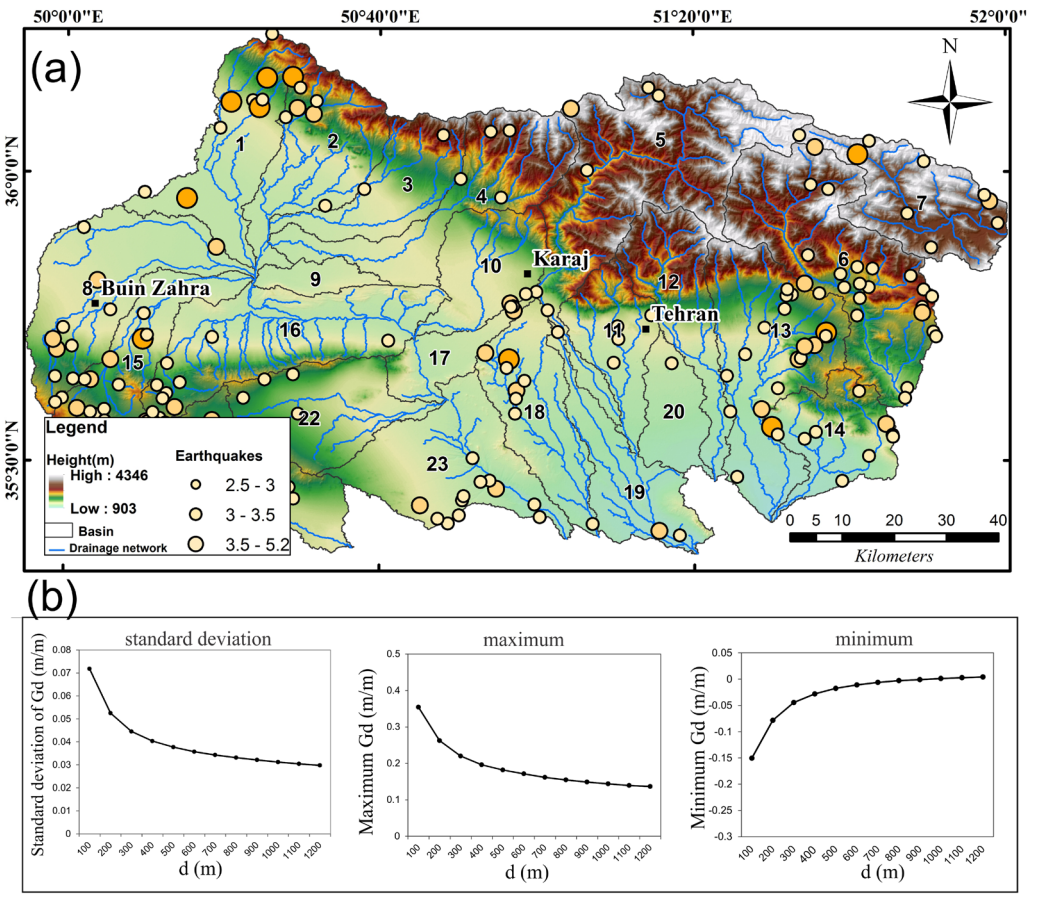

Figure 2. (a) Digital elevation model (DEM) (http://www.gdem.aster.ersdac.or.jp) showing drainages of 23 sub-basins (Earthquakes data of the study area from www.irsc.ut.ac.ir). (b) The statistical values of Gd (d = 100–1200 m) in the study area.

Oguchi, 2006, 2009). There are two types of the local gradient and the trend gradient for the river. In this study, the border between the local and gradient was considered to be 1200 m. Calculations show the decrease of Gd with the increase of d for d < 1200 m in the local gradient, as well as the maximum values and standard deviation decrease with the increase of d, and the minimum values of Gd are negative in short distances, which are related to local DEM errors. The values of the Gd indicate the changes in the gradient of the river, which are high in local distances, and decrease with the increase of the distance, and the curve becomes a longitudinal profile of the river (Hayakawa and Oguchi, 2006, 2009).

The knickpoint may also develop as an unbalanced steepening in response to a relative fall in base level. Such transient state in bedrock rivers are commonly triggered by sea-level fall and surface uplift, these steepenings are interpreted as knickpoints and this is confirmed by logarithm gradient-distance plots (Bishop et al., 2005). In order to investigate the knickpoints created by tectonic activity, we prepared a natural logarithm gradient and elevation diagrams (Figure 3a) using the Gd value.

The relative slope of the riverbed can be presented by Rd, which shows the rate of gradient change with increasing d (Hayakawa and Oguchi, 2006). The quantitative value of transition for each measurement point is derived from a regression line fitted to the relation between Gd and d.

After the Gd calculation for each sampling point with varying d, the quantitative value of transition from a regression line is fitted to Gd-d relation. The regression equation for the relationship between Gd and d is:

$$Gd = ad + b,$$

where a and b are coefficients of the linear regression. Rd, the rate of gradient change with increasing d and an indicator of relative steepness, is the negative slope of regression line:

$$Rd = -a.$$

The curve of Rd along the river shows fluctuations, in which relatively steep segments correspond to large values of Rd. Here, Gd with a d range of 200–1200 m is considered for calculating the Rd value for all the streams. Considering that the threshold value of Rd was determined equal to 5.7×10^{-6}; therefore, the river sections with Rd greater than this value were determined as knickpoints (Hayakawa and Oguchi, 2006). According to the values of Gd measured in the previous step, the values of Rd were measured using the defined MATLAB code. The final output was the diagram of Rd along the river with the threshold value of the relative steepness. Further, to reduce the ambiguity, minimum height to identify knickzones was set as 20 m. Hence, the margin of error in identifying the ambiguous knickzones was narrowed even if they have Rd values larger than 5.7×10^{-6} m^{-1}.

3.3. Channel steepness index (k_{sn})

Channel steepness index (k_{sn}) is one of the characteristics of rivers that can be extracted from digital elevation models (DEMs) using the codes defined in MATLAB. According to Flint's law (Flint, 1974), the river profile is depicted in steady state as follows:

$$S = k_S A^{-\theta},$$

where S is local channel slope, A is contributing drainage area, k_S is channel-steepness index, and θ is the concavity index (e.g., Flint, 1974; Whipple and Tucker, 1999; Snyder et al., 2000; Kirby et al., 2003). Because of the strong relationship between channel concavity θ and the steepness index k_S, any variation or uncertainty in determined θ can lead to large k_S variations. In order to compare the streams of different basins precisely, k_S value is normalized to a reference concavity ($\theta_{ref} = 0.45$) (Kirby and Whipple, 2001). Assuming a reference concavity θ_{ref}, the normalized channel steepness k_{sn} becomes:

$$S = k_{sn} A^{-\theta ref}.$$

We obtained from the slope area regression of all studied rivers an average regional convexity $\theta_{ref} = 0.47$. This average value is similar to the $\theta_{ref} = 0.45$, which has been considered as an equilibrium value in similar geomorphological studies (e.g., Snyder et al., 2000; Wobus et al., 2006; DiBiase et al., 2010; Yildirim et al., 2011; Kirby and Whipple, 2012; Haghipour and Burg, 2014; Martins et al., 2017; Babaei et al., 2020). Therefore, we used $\theta_{ref} = 0.45$ to measure the normalized k_{sn}. To identify the knickpoints that have formed in connection with the region faults, the k_{sn} distribution diagram was obtained for all the rivers. In the parts where the rivers are affected by the faults, the value of this index is high, which is consistent with the field evidence. The parts of the rivers that are affected by faults and have high k_{sn} values were identified as Tk_{sn} (Figure 3b).

As shown in Figure 3b, to identify the TFKs, the k_{sn} distribution plots were fitted with the longitudinal profile of the rivers, which shows the correspondence of all the knickpoints. knickpoints that corresponded to Tk_{sn} were identified as TFKs and lithological knickpoints were spared. The smooth profile and logarithm slope area diagram was obtained to evaluate the TFKs that convex-up shape in the longitudinal profile, breaks in logarithm slope-area diagram with the increase of k_{sn} value below knickpoints on the slope area plots were consistent with the location of TFKs (Figure 3c).

By plotting the slope-distance of the natural logarithm and the distance of the height-distance of the natural logarithm, it was determined that the slope changes at the place of the TFKs (Figure 3a). The transversal passage of the river through various lithology with different strength level of the rocks causes the formation of knickpoints (Stock and Montgomery, 1999). In addition to tectonic and lithological factors, factors such as dam construction

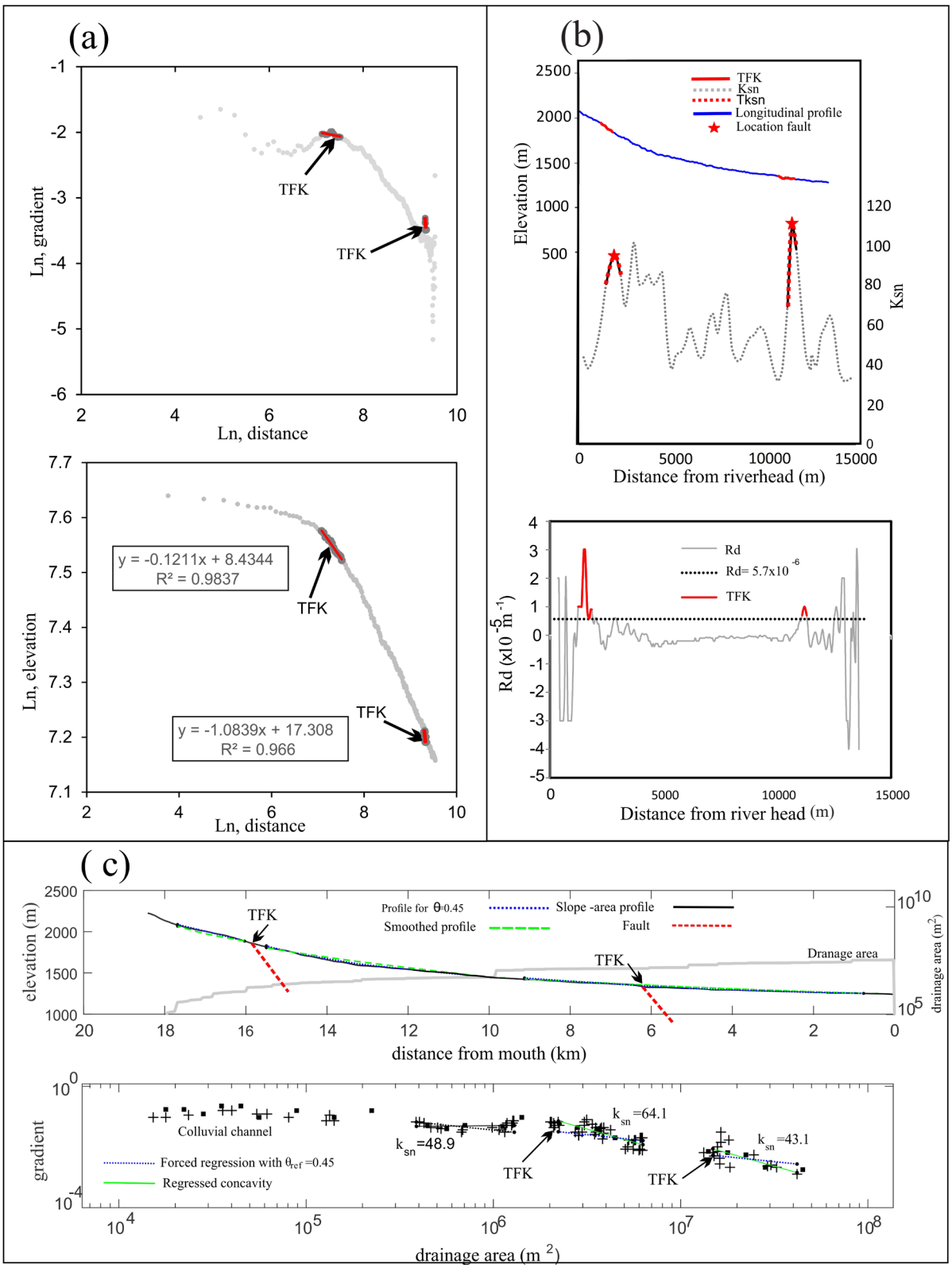

Figure 3. Evidence of identified TFKs from the river basin 1: (a) the diagrams of natural logarithm gradient-distance and natural logarithm elevation-distance, (b) the longitudinal profile, Rd, k_{sn}, and Tk_{sn} diagrams, and (c) the smooth profile and logarithm slope-area diagram.

can cause knickpoints. In this study, several knickpoints were identified at the outlet of the dams, which were ignored. Figure 4 shows the relationships between different factors in the formation of knickpoints, the frequency of knickpoints computed for each class of elevation (height of knickpoints), distance from the riverhead, altitude, stream gradient, and lithology was also considered in all these diagrams. These diagrams indicate that knickpoints are more number in steep upper reaches.

4. Results

The analysis of streams identified 332 knickpoints by using stream gradient in study area. A summary of the overall statistical values of knickpoints is shown in Table 1.

The mean height is 49.3 m, the mean length is 306.1 m, and the mean relative steepness is 3.6×10^{-5} m^{-1}. The knickpoint properties for all 23 drainage basins display that knickpoint generation is related to lithology and tectonic activity. The rock resistance level is classified according to the rock types shown in Figure 1 and field observations: very low (alluvial deposits), low (older alluvial fan deposit, weakly cemented Conglomerates), moderate (shale, phyllite, schist, marl, gypsum, and tuff), high (sandstone, dolomite, limestone, and hard conglomerate) and very high (volcanic and plutonic rocks).

According to longitudinal river profiles, the knickpoints are more number between elevations 1300 and 2500 m (Figure 4a), knickpoints underlain by with high and moderate strength rocks are more number at height >50 m (Figure 4a), more number of the knickpoints underlain by moderate strength rocks are located more than 20 km from the riverhead location and knickpoints underlain by low strength rocks have a stream gradient <0.1 mm^{-1} (Figure 4a). These anomalies offer that the rivers have been affected by tectonic activity.

Figure 4b shows that small knickpoints can be created in any part of the rivers, whereas large knickpoints, >100 m in height or >500 m in length, are observable in upper reaches with >1500 m altitude, <8 km upstream distance. However, the knickpoints that have high height, length and steep are usually formed near the river head and also the knickpoints gradient and relative steepness (Rd) decrease with increasing distance upstream.

The mean of knickpoints characteristics according to the lithology strength related to the area where knickpoint is formed are summarized in Table 2. The average height, length, gradient and relative steepness of the knickpoints for hard and medium lithology strength are all larger than those for the other strength types.

The lithology formed knickpoints (LFKs) created in the area are shown in Figure 5. These knickpoints are created due to the various resistivity values of rock units against river cutting. The mean length of LFKs is 327.3 m, the mean height is 52.14 m, the mean relative steepness is 3.95×10^{-5} m^{-1}. The large LFKs are located at the boundaries of high strength and moderate to very low resistance (Figure 5).

The effects of the rock strength on the frequency of knickpoints (Figure 4a) suggest that TFKs underlain by moderate and low strength rocks and are located more than 20 km from the riverhead location in the study area, and most of the height and steep knickpoints are underlain by high and moderate strength rocks (Figure 4a).

In this paper, by analyzing the diagrams obtained from the results of stream gradient and river profile and matching them together, the normalized channel steepness index (k_{sn}) and Gd index for all rivers in the area were calculated (Figure 3), and the position of the TFKs were identified. The positions of the TFKs correspond with the study area faults and they are mainly have formed in high relief areas and in specific elevation changes, which the uplift rate can be related to the recent tectonic activity. More than 170 TFKs were extracted in the study area, which are shown in Figure 5 on the resistance of rock unit's map. The height and length of TFKs were examined and the changes in the length and height of TFKs related to the five main faults of the area were displayed on the graph (Figure 6).

The number of TFKs created in connection with Mosha Fault is more than other faults. The height of TFKs is 20–559 m and the length of TFKs is 0.1–1.6 km on the Mosha Fault. TFKs show more height changes than the changes in length, can be known as high-altitude kind. The lowest changes in the height and length of the TFKs are related to the Ipak fault, which is 26–29 km in height and 0.21–0.28 km in length (Figure 6).

The location of TFKs in strike some of the faults were confirmed from the high-resolution satellite images of Google Earth and field studies (Figure 7).

5. Discussion

There is a significant relationship between the distribution of TFKs, rock units uplift and the location of faults in the study area (Figure 5). Oblique shortening movements across the Alborz Belt in response to the Arabia-Eurasia collision since 12 Ma has occurred and the Alborz Mountains along its faults were uplifted (e.g., Allen et al., 2003; Ritz et al., 2006; Guest et al., 2006). The measured shortening rate in the south Alborz Belt is about 3 mm/year (Vernant et al., 2004; Djamour et al., 2010). Since most of the major faults in the Central Alborz Belt have reverse kinematics (e.g., Allen et al., 2003; Guest et al., 2006; Yassaghi and Madanipour, 2008), the activity of these faults is an effective factor in the formation of knickpoints (Hayakawa and Oguchi, 2006). Also, during tectonic activity some knickpoints can be created near the mountain foot (Reneau, 2000). Therefore, the creation of knickpoints along

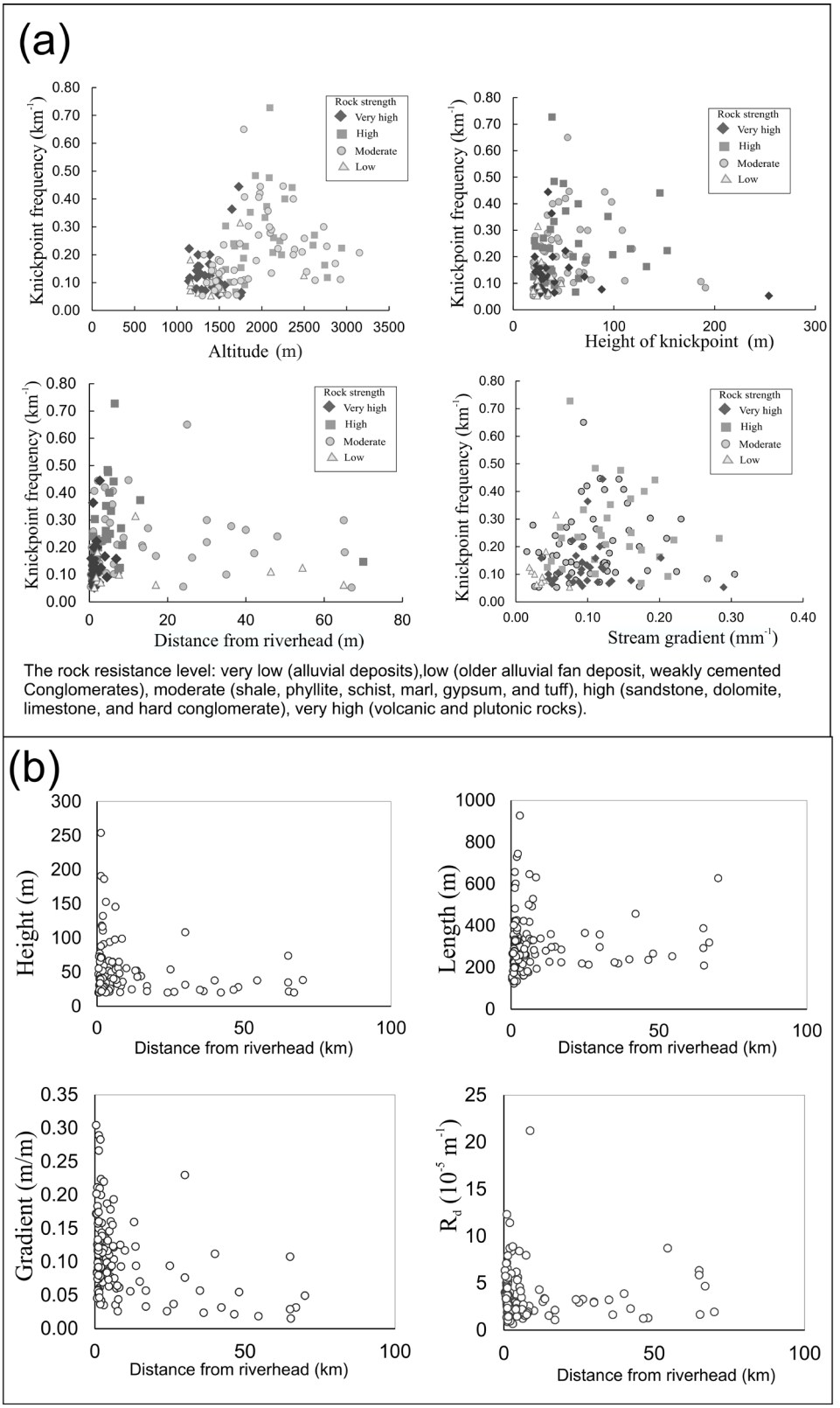

Figure 4. (a) Knickpoint frequency for each rock strength level against altitude, height of knickpoint, distance from riverhead and stream gradient. (b) Relationships between parameters of knickpoints (height, length, gradient and relative steepness (Rd)) and distance from riverhead.

Table 1. General knickpoints statistics.

	Rd ($\times 10^{-5}$)	Height (m)	Length (m)	Stream gradient (mm^{-})
Maximum	21.20	254	927	0.30
Minimum	0.66	20	123	0.02
Mean	3.63	49	306	0.11
Standard deviation	2.72	37	136	0.06

Table 2. Mean values of knickpoints form parameters for each rock strength type.

Rock strength	Height (m)	Length (m)	Gradient (mm^{-1})	Rd ($\times 10^{-5}$)
High	61	348	0.13	3.68
Moderate	53	314	0.11	3.74
Very high	40	278	0.10	3.54
Low	29	272	0.04	3.3

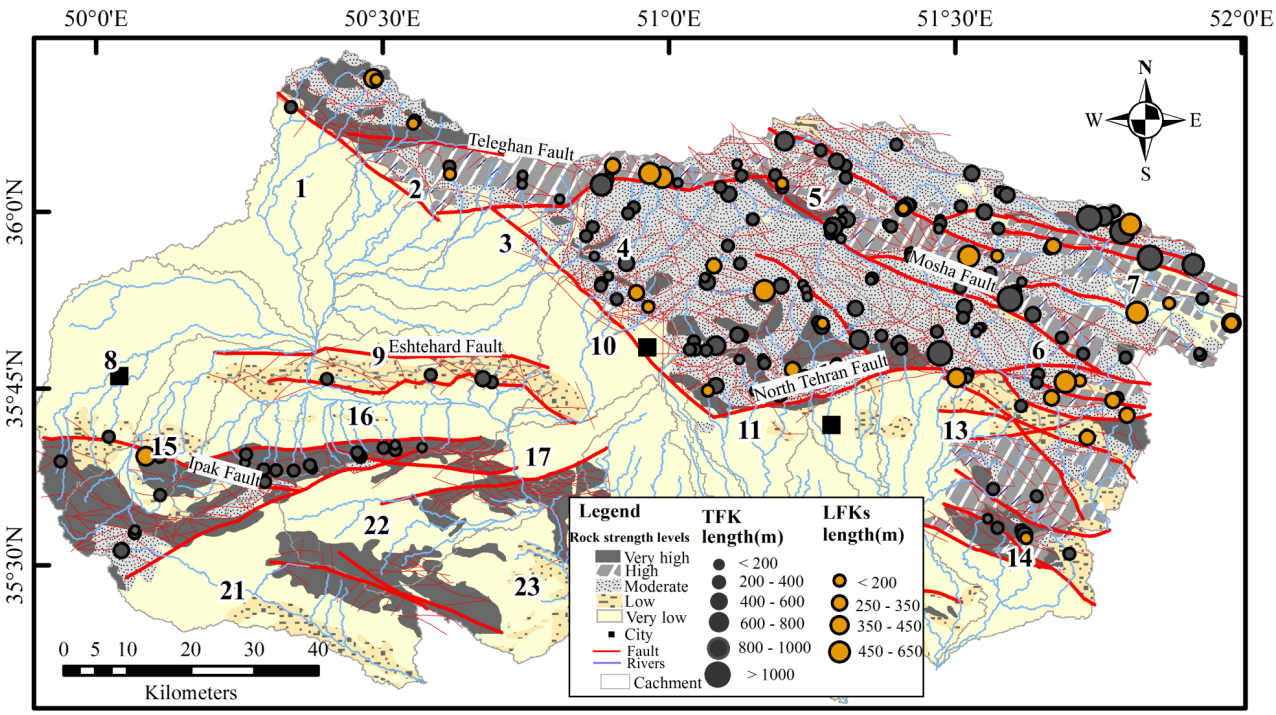

Figure 5. The distributions of TFKs and LFKs in in the study area.

faults and in the longitudinal profile of rivers can be considered as evidence for identifying new tectonic activities in each region. In this study, the vertical movements (uplift or subsidence) of the Central Alborz Belt obtained by quantitative investigation of TFKs on the study area faults are comparable with the results of previous studies carried out using GPS (Vernant et al., 2004; Djamour et al., 2010). The analysis of exact leveling data in Central Alborz Belt and study on the vertical movement from the north to the south shows the greater uplift in the southern flank (study area) (10.4 ± 0.9 mm) than its northern flank (6.3 ± 0.9 mm), in the same times (Saberi et al., 2017). It indicates

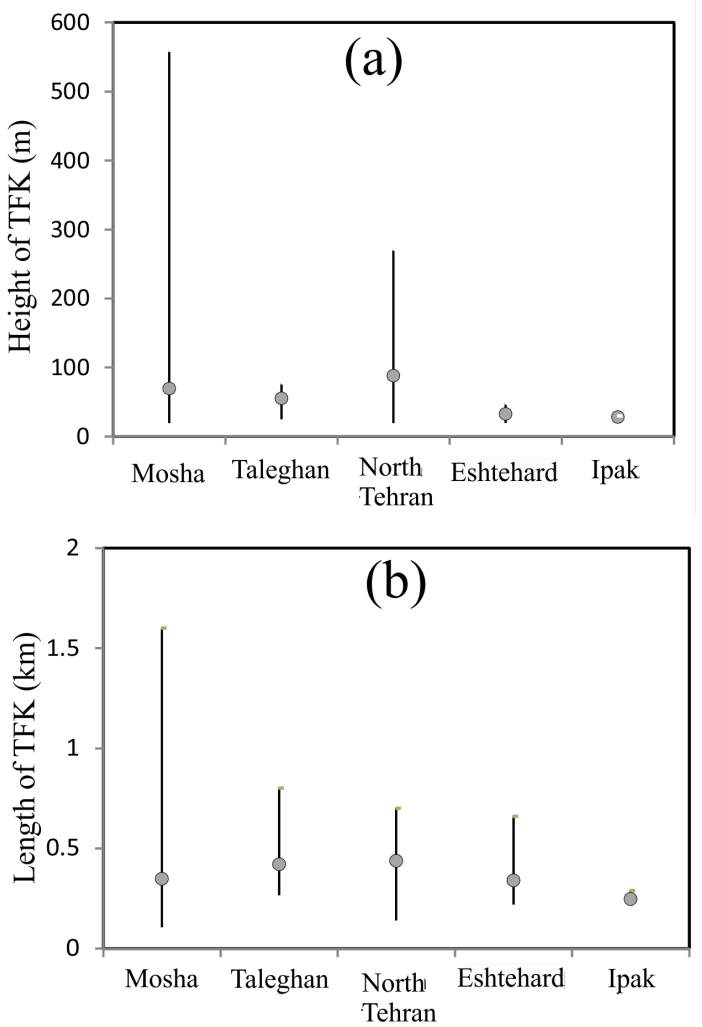

Figure 6. The general parameters of TFKs for the main faults of the study area: (a) height and (b) length. Grey circles indicate the average and black lines show the standard deviation.

a young deformation development in the Central Alborz Belt toward its southern hillside (Saberi et al., 2017). The occurrence of several historical and instrumental earthquakes on the main faults of the area such as the north Tehran, Mosha, Taleghan, Ipak and Eshtehard faults and other recent activity evidences like morphotectonics data and paleoseismological analysis (Nazari, 2006; Nazari and Ritz, 2008; Nazari et al., 2009; Ritz et al., 2012) show the importance of identifying TFKs to investigate the recent tectonic activities. The location of the extracted TFKs, their frequency and connection with the faults indicate the active parts of the fault, the rise and change of the slope of the rivers (Figure 5).

The channel steepness index (k_{sn}) of the channel increases uniformly with the increase of rock uplift relative to base level or erosion rate (DiBiase et al., 2010; Duvall et al., 2004; Kirby and Whipple, 2001; Kirby et al., 2003). The parts of the river that are located on the segments the North Tehran, Mosha, Taleghan, Ipak and Eshtehard faults show high amounts of k_{sn}; therefore, the identified TFKs were determined based on the Tk_{sn} overlap on the knickpoints location that extracted using Gd. The knickpoints on active faults that have the high values of k_{Sn} (Tk_{sn}) can represent TFKs in the area. In this study were used natural logarithm gradient-distance, natural logarithm elevation-distance, smooth profile and logarithmic slope-area dia-

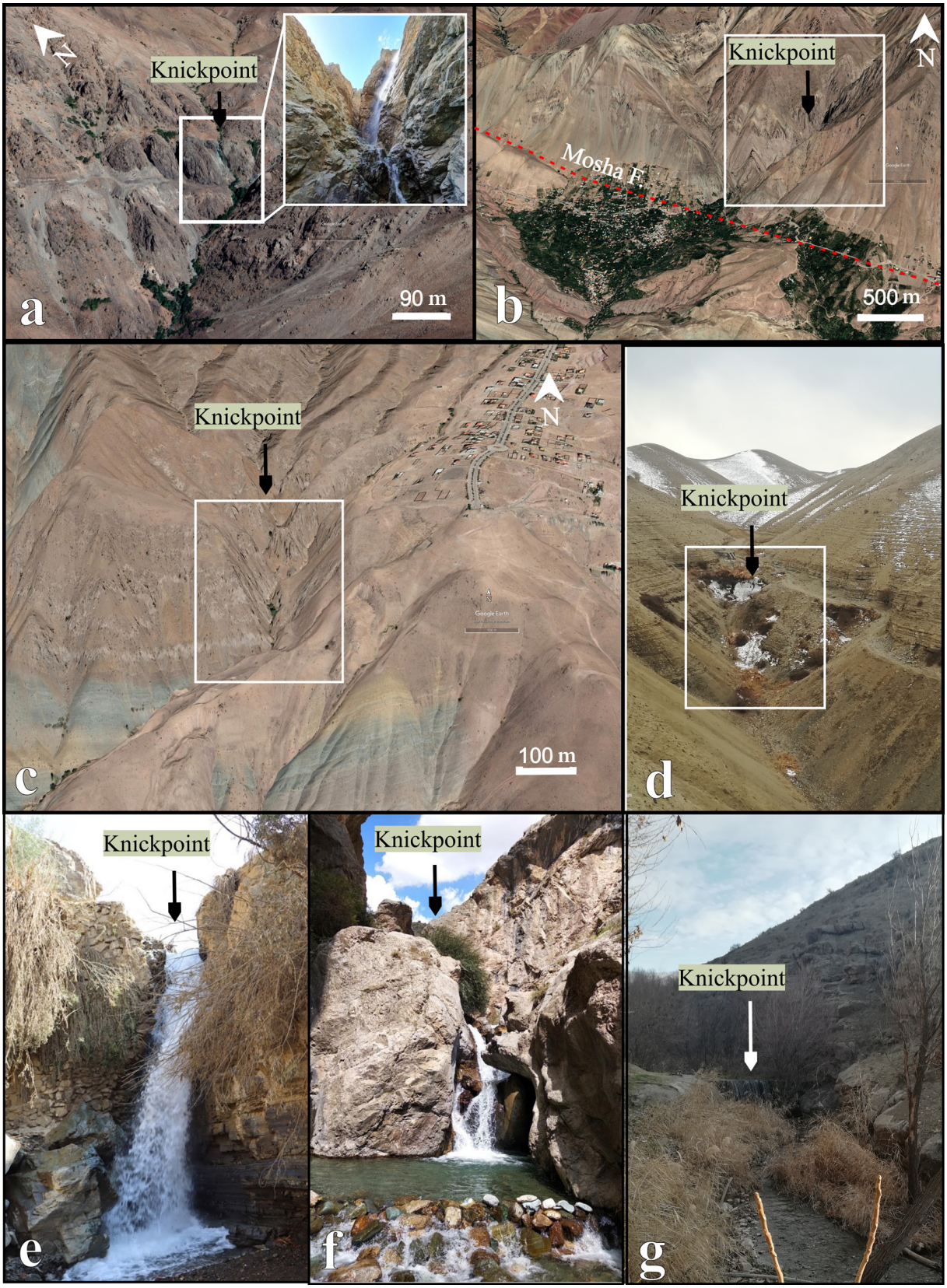

Figure 7. The examples of TFKs of Google Earth images (a–c), and field observations (d–g).

gram for more detailed examination of the anomalously steep segments of the streams are mainly found in strike tectonic lineaments (Figure 3). The natural logarithm elevation-distance diagram and the natural logarithm gradient-distance diagram indicate elevation changes and irregular outliers at the location of active faults creating TFKs (Figure 3a).

The results obtained from the examination of different charts in all subbasins of the studied area indicated that the fault segments are aligned with anomalies, where TFKs are located. Changes in gradient, length and height of TFK in different faults were investigated. In most of the rivers that are located on the North Tehran, Mosha and Taleghan faults in the north and the Eshtehard and Ipak faults in the south and southwest of the area, the TFKs were extracted on the fault segments (Figure 5). The characteristics (height, length) of the TFKs on the main faults are shown on the diagram in Figure 6.

Figure 8a shows the longitudinal profile of the river and k_{sn} values in basin 6 on the Mosha Fault which is of special importance for study due to strong historical seismicity and obvious morphotectonic evidence (Ritz et al., 2006). The changes of k_{sn} values are consistent with the knickpoints, which indicate TFKs related to these faults. TFKs associated with Mosha Fault has the largest length and height, which is also consistent with the increase in Rd values (Figure 8a) and gradient changes (Figure 8b), on the river longitudinal profile and logarithm slope-area diagram (Figure 8c), the slope-break knickpoints are well observed that confirms large TFKs on the Mosha Fault (Figure 8c). Large TFKs are located in the west segment of the Mosha Fault, and the assessment of the uplift rate for the major faults in Central Alborz also indicates an increase in vertical uplift in the western part of the main faults in Central Alborz, such as Mosha Fault (Saberi et al., 2017). The rate of uplift in the hanging wall of the Mosha Fault is 0.921 ± 0.283 mm/year in the west and 0.508 ± 0.228 mm/year in the east (Saberi et al., 2017), and existence of the extracted TFKs in segments of the western and eastern of Mosha Fault is completely consistent with these uplifts (Figure 5). Our suggestion is that the formation of these TFKs and their matching with fault segments indicate recent tectonic activities in the area.

The slope-break knickpoints in the river longitudinal profile (Figure 9c) and the disordered outliers on the gradient-distance diagrams (Figure 9b) at the location of TFKs related to the North Tehran Fault suggest that these TFKs directly related to the North Tehran Fault, which is one of the active faults in the study area (Ritz et al., 2006; Ritz et al., 2012) and has caused some TFKs (Figure 9a) in basin 12. The formation of the knickpoints on the North Tehran Fault with high values of k_{sn} corresponds to the Rd values (Figure 9a).

The Taleghan Fault is a major active fault of the Central Alborz that has left-lateral and normal components of movements (Nazari et al., 2009). With studies the morphological and paleoseismological data, the minimum vertical and horizontal slip rate along the Taleghan Fault has been estimated to be approximately 0.5 mm/year and 0.6–1.6 mm/year, respectively (Nazari et al., 2009). The presence of several TFKs on the eastern part of the fault corresponds to its vertical movement component. The activity of the eastern segment of the Taleghan Fault in one of the rivers of basin 5 has created three TFKs. The TFKs in strike the Taleghan Fault have a length of 620–380–450 m. The location of the peak of k_{sn} and the values of Rd (Figure 10a) corresponds to the position of the slope-break in the river longitudinal profile (Figure 10c), also the disordered outliers in gradient-distance plots and the elevation changes in the elevation-distance plots are compatible with the segments of this fault and indicate TFKs (Figure 10b).

The Eshtehard and Ipak faults have reverse and left-lateral components of movements (Ambraseys, 1963; Berberian, 1983; Berberian et al., 1993) and are main structures in the west and southwest of the study area. Due to the history of seismicity in this part of the study area, the most important of which is the 1962 Buin Zahra earthquake (Ms 7.2) (Ambraseys, 1963), it is necessary to investigate the knickpoints related to the faults and try to recognize the active segments of the faults. The position of the TFKs created on these faults corresponds with the increase of k_{sn} values (Figures 11a and 12a) and indicates the active segments of them. The longitudinal profile of river, logarithm slope-area diagram (Figures 11c and 12c) and the disordered outliers at the location of TFKs on the gradient-distance diagrams (Figures 11b and 12b) confirmed the connection of these TFKs with Eshtehard and Ipak faults.

6. Conclusion

To investigate the response of gradients changes in the longitudinal profile of the rivers to the deformations resulting from the recent tectonic activities, using the normalized channel steepness index (k_{sn}) and Gd index, the tectonically formed knickpoints (TFKs) in the south of Central Alborz area were identified and confirmed by field observations.

The results showed that the area has more than 300 knickpoints, which are scattered in the area and are mainly located along the active segments of faults in the south of Central Alborz Belt. Examining the results of longitudinal profile, logarithm slope-area plots, and natural logarithm gradient-distance plots confirms the correspondence of the TFKs position with the active fault segments and shows their tectonic origin.

The characteristics of the extracted TFKs for the main faults of the study area confirmed that the TFKs show more height changes than the changes in length in the Mo-

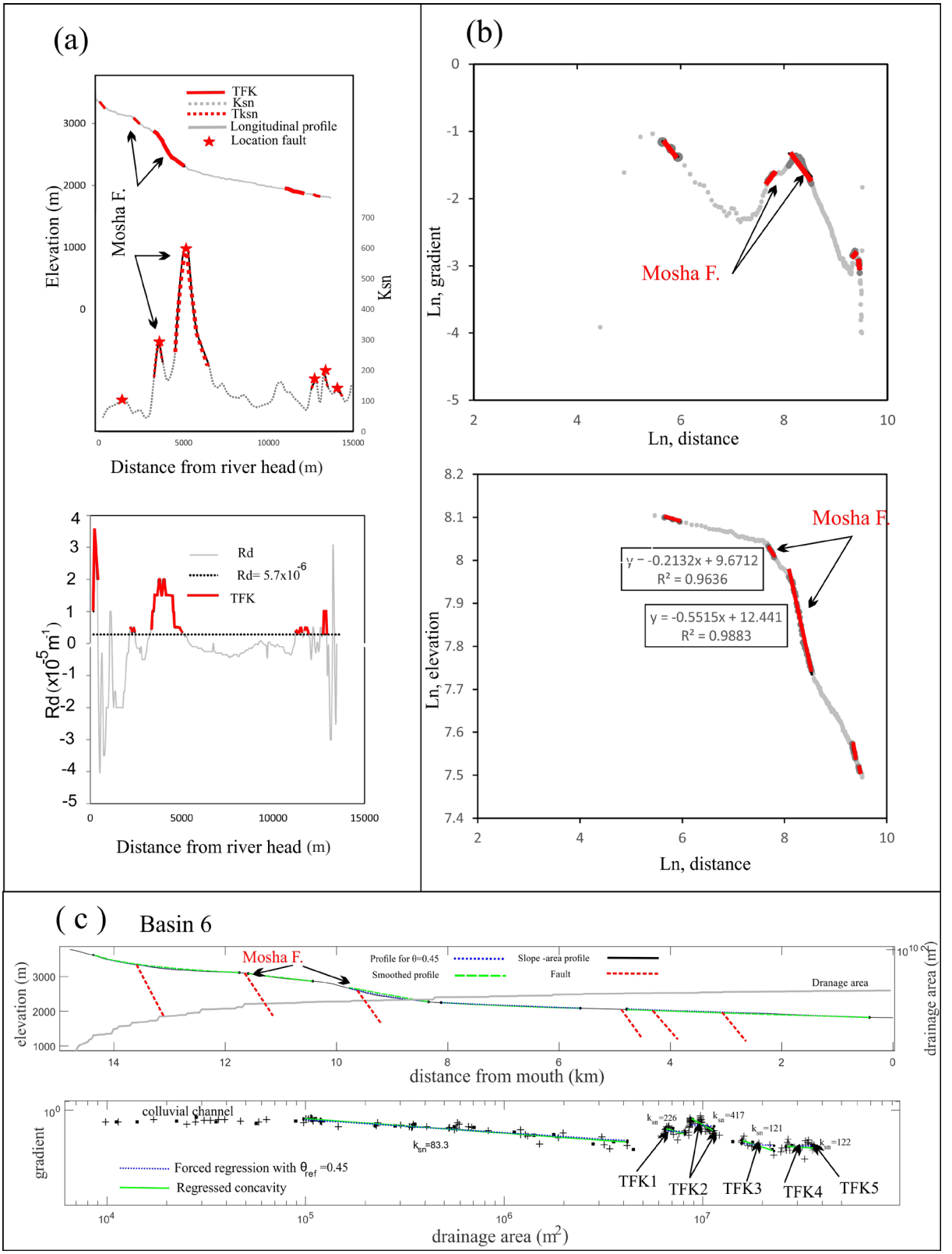

Figure 8. The position of TFKs created by the Mosha Fault (This is the main river of subbasin 6.): (a) the longitudinal profile, Rd, k_{sn}, and T k_{sn} diagrams, (b) the diagrams of natural logarithm gradient-distance and natural logarithm elevation-distance, and (c) the smooth profile and logarithm slope-area diagram.

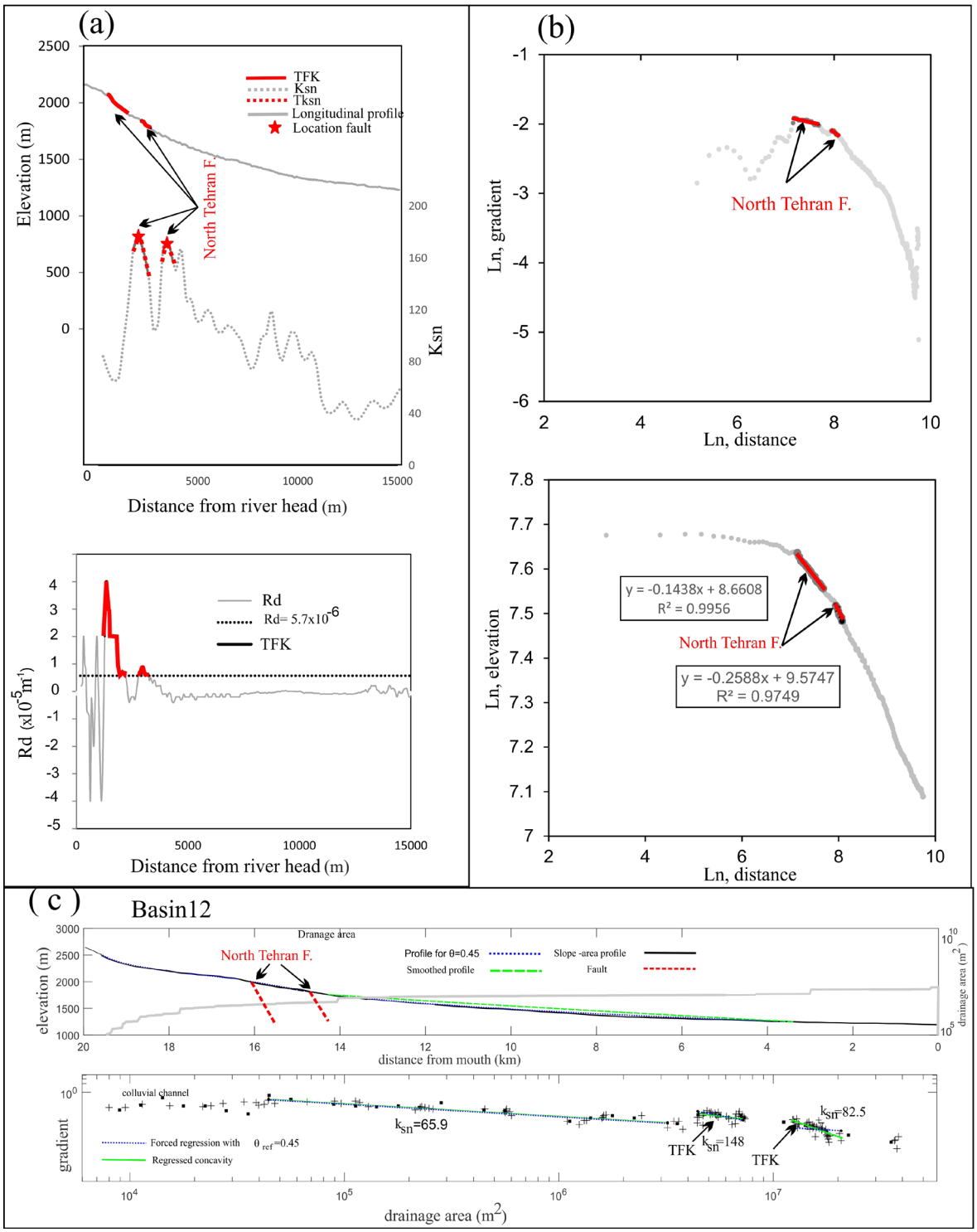

Figure 9. The position of TFK created by the North Tehran Fault (This is the main river of subbasin 12.): (a) the longitudinal profile, Rd, k_{sn}, and Tk_{sn} diagrams, (b) the diagrams of natural logarithm gradient-distance and natural logarithm elevation-distance, and (c) the smooth profile on the raw profile and logarithm slope-area diagram.

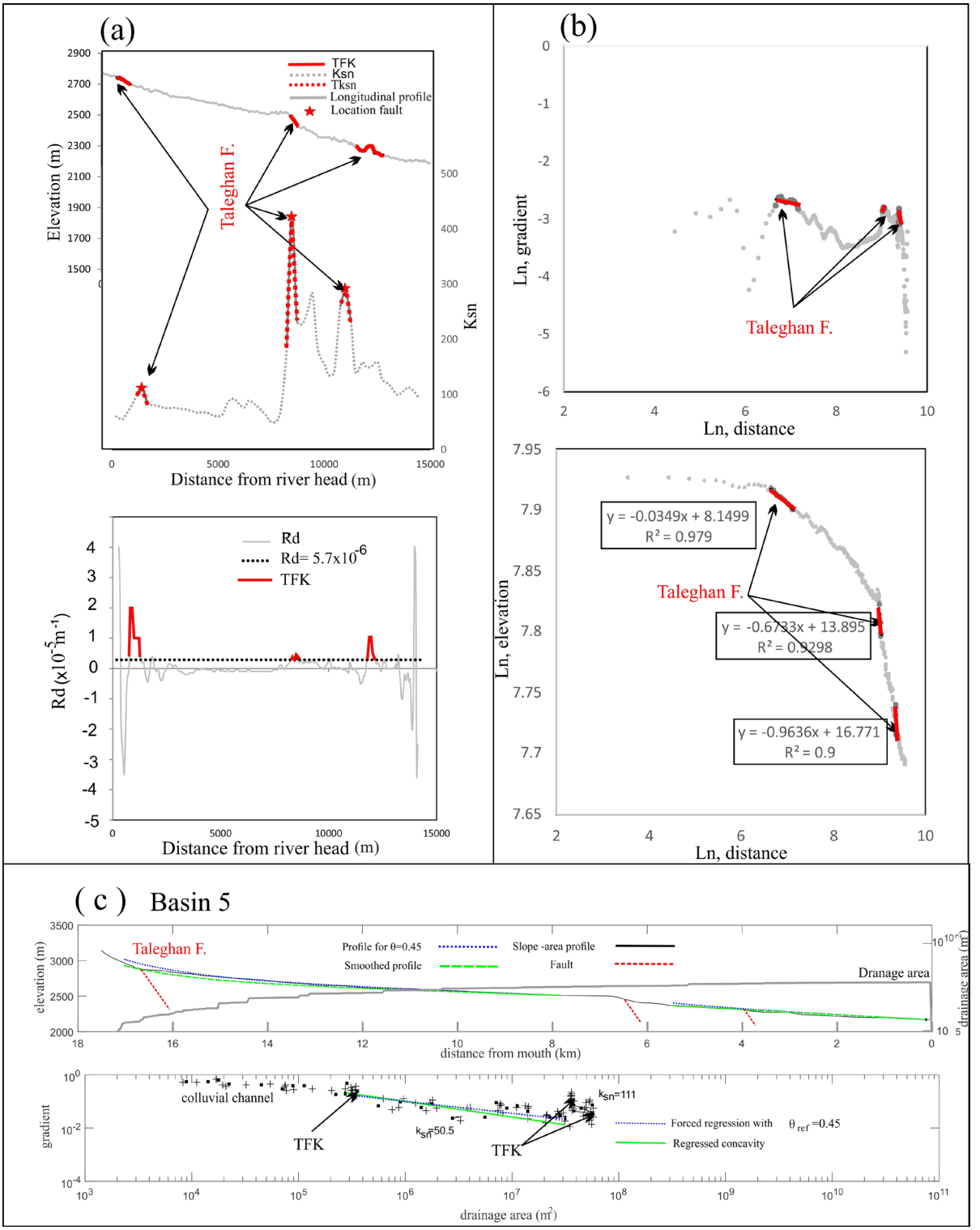

Figure 10. The position of TFK created by the Taleghan Fault (This is the main river of subbasin 5.): (a) the longitudinal profile, Rd, k_{sn}, and Tk_{sn} diagrams, (b) the diagrams of natural logarithm gradient-distance and natural logarithm elevation-distance, and (c) the smooth profile on the raw profile and logarithm slope-area diagram.

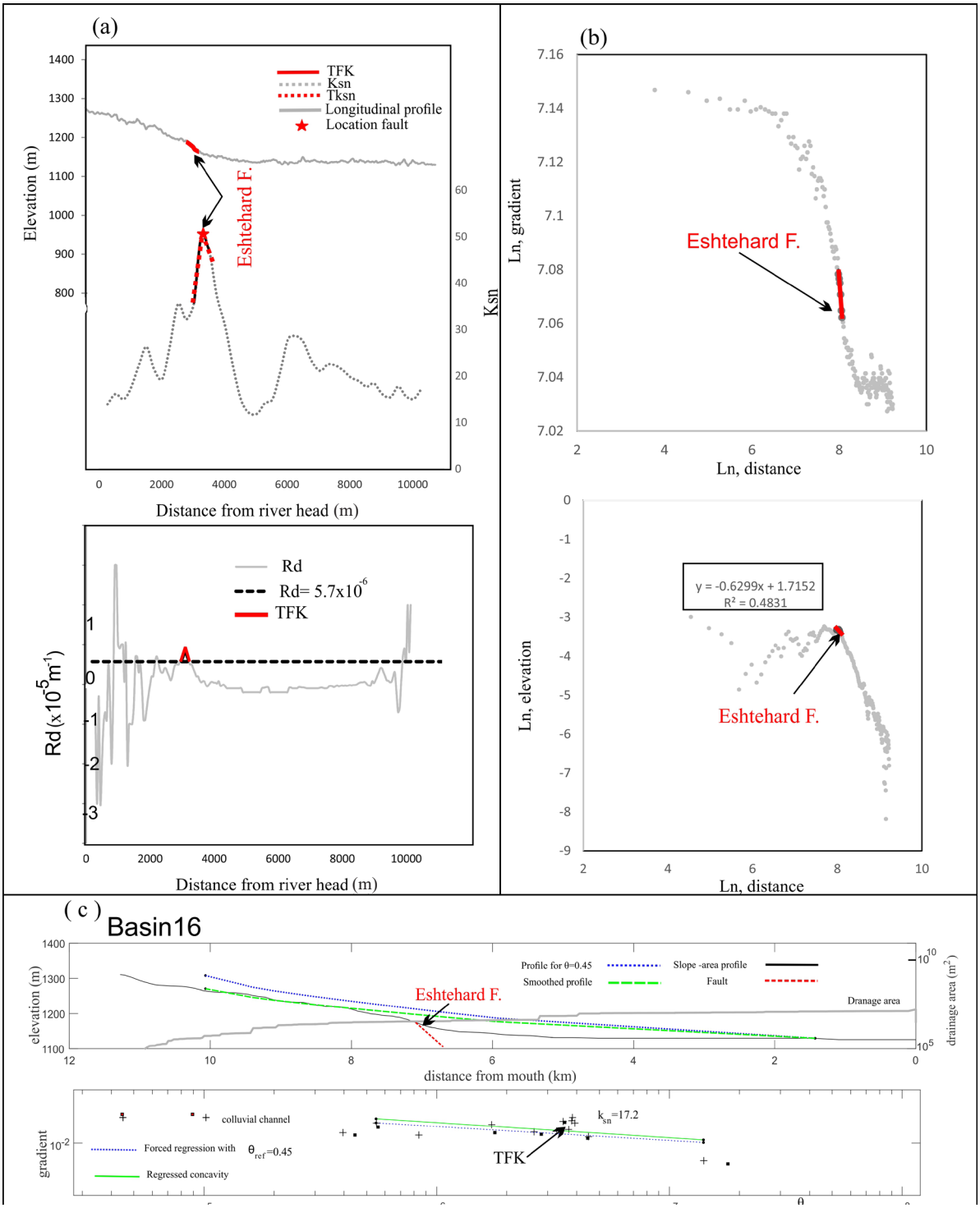

Figure 11. The position of TFK created by the Eshtehard Fault (This is the main river of subbasin 16.): (a) the longitudinal profile, Rd, k_{sn}, and Tk_{sn} diagrams, (b) the diagrams of natural logarithm gradient-distance and natural logarithm elevation-distance, and (c) the smooth profile on the raw profile and logarithm slope-area diagram.

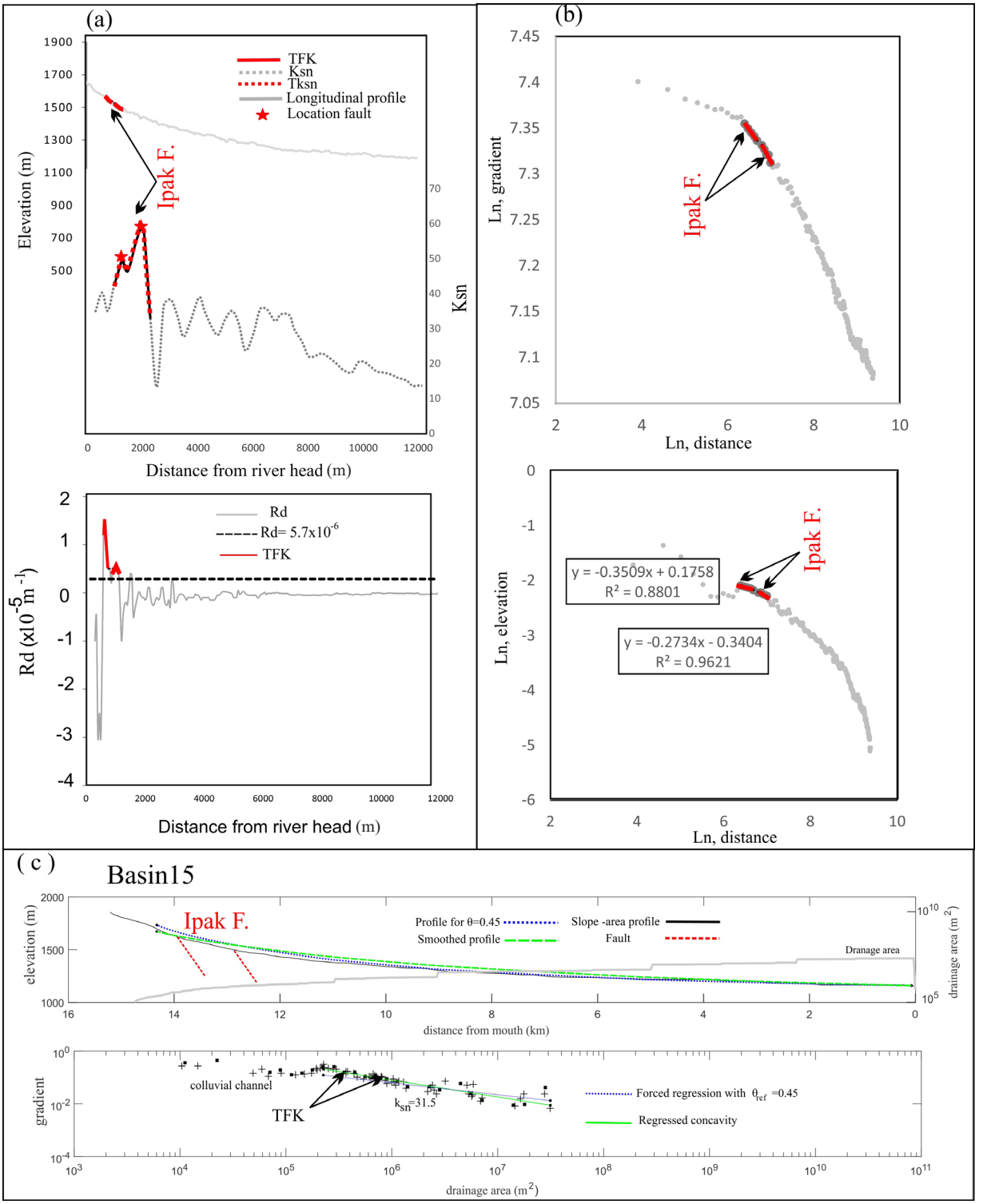

Figure 12. The position of TFK created by the Ipak Fault (This is the main river of subbasin 15.): (a) the longitudinal profile, Rd, k_{sn}, and Tk_{sn} diagrams, (b) the diagrams of natural logarithm gradient-distance and natural logarithm elevation-distance, and (c) the smooth profile on the raw profile and logarithm slope-area diagram.

sha and North Tehran faults; therefore, they can be known as high-altitude ones. And the TFKs along the Taleghan and Eshtehard faults show more changes in the length of knickpoints and can be regarded as long-distance TFKs. TFKs related to Ipak Fault have the smallest length and height.

The obtained results in this research showed that the identification of knickpoints in the south of the Central Alborz Belt can be used to investigate recent tectonic activities and seismic hazards in the future.

Acknowledgments

This research has been done in accordance with the PhD dissertation at University of Isfahan. We thank the Department of Geology of the University for providing the necessary facilities for field surveys. First author would also like to thank Shima Babaei for their great help.

References

Aghanabati A (2004). The Geology of Iran. Tehran, Iran: Geological Survey of Iran (In Persian).

Alavi M (1996). Tectonostratigraphic synthesis and structural style of the Alborz mountain system in northern Iran. Journal of Geodynamics 21 (1): 1-33. https://doi.org/10.1016/0264-3707(95)00009-7

Allen MB, Ghassemi MR, Sharabi M, Qoraishi M (2003). Accommodation of late Cenozoic oblique shortening in the Alborz Range, northern Iran. Journal of Structural Geology 25: 659–672. https://doi.org/10.1016/S0191-8141(02)00064-0

Ambraseys NN (1963). The Buyin-Zara (Iran) earthquake of September, 1962 a field report. Bulletin of the Seismological Society of America 53 (4): 705–740. https://doi.org/10.1785/BSSA0530040705

Ambraseys NN, Melville CP (1982). A History of Persian Earthquakes. Cambridge University Press, New York. 46, 219.

ASTER Global Digital Elevation Model (GDEM) (2022). Website https://www.jspacesystems.or.jp/ersdac/GDEM

Babaei Sh, Dehbozorgi M, Hosseiniasl M, Hakimi Asiabar S (2020). New insights into the effect of the quaternary fault activity on river knickpoints in the Central Alborz (Iran). Quaternary International 562: 104-120. https://doi.org/10.1016/j.quaint.2020.09.025

Ballato P, Nowaczyk NR, Landgraf A, Strecker MR, Friedrich A et al. (2008). Tectonic control on sedimentary facies pattern and sediment accumulation rates in theMiocene foreland basin of the southern Alborzmountains, northern Iran. Tectonics 27 (6): 1–20. https://doi.org/10.1029/2008TC002278

Ballato P, Mulch A, Landgraf A, Strecker MR, Dalconi MC et al. (2010). Middle to late Miocene Middle Eastern climate from stable oxygen and carbon isotope data, southern Alborz mountains, N Iran. Earth and Planetary Science Letters 300 (1-2): 125-138. https://doi.org/10.1016/j.epsl.2010.09.043

Ballato P, Uba CE, Landgraf A, Strecker MR, Sudo M et al. (2011). Arabia-Eurasia continental collision: Insights from late Tertiary foreland-basin evolution in the Alborz Mountains, northern Iran. Geological Society of America Bulletin 123 (1-2): 106-131. https://doi.org/ 10.1130/B30091.1

Ballato P, Landgraf A, Schildgen TF, Stockli DF, Fox M et al. (2015). The growth of a mountain belt forced by base-level fall: tectonics and surface processes during the evolution of the Alborz Mountains, N Iran. Earth and Planetary Science Letters 425: 204–218. https://doi.org/10.1016/j.epsl.2015.05.051

Berberian M (1983). The southern Caspian: a compressional depression floored by a trapped, modified oceanic crust. Canadian Journal of Earth Sciences 20: 163–183. https://doi.org/10.1139/e83-015

Berberian M, Ghorashi M, Argangravesh B, Mohajer Ashjaie A (1985). Seismotectonic and Earthquake fault hazard investigations in the Tehran region (In Persian). Tehran, Iran: Geological Survey and Mineral Exploration of Iran.

Berberian M, Ghorashi M, Arjangravesh B, Mohajer Ashjaie A (1993). Seismotectonic and earthquake fault hazard investigations in the great Ghazvin Region (In Persian). Tehran, Iran: Geological Survey and Mineral Exploration of Iran.

Bishop P, Hoey TB, Jansen JD, Lexartzaartza I (2005). Knickpoint recession rate and catchment area: the case of uplifted rivers in eastern Scotland. Earth Surface Process Landforms 30 (6): 767–778. https://doi.org/10.1002/esp.119

Boulton SJ, Stokes M, Mather AE (2014). Transient fluvial incision as an indicator of active faulting and Plio-Quaternary uplift of the Moroccan High Atlas. Tectonophysics 633: 16–33. https://doi.org/10.1016/j.tecto.2014.06.032

Castillo M, Bishop P, Jansen JD (2013). Knickpoint retreat and transient bedrock channel morphology triggered by base-level fall in small bedrock river catchments: The case of the Isle of Jura, Scotland. Geomorphology 180–181: 1-9. https://doi.org/10.1016/j.geomorph.2012.08.023

Crosby B, Whipple K (2006). Knickpoint initiation and distribution within fluvial networks: 236 waterfalls in the Waipaoa River, North Island, New Zealand. Geomorphology 82 (1–2): 16–38. https://doi.org/10.1016/j. geomorph.2005.08.023

Demoulin A, Mather A, Whittaker A (2017). Fluvial archives, a valuable record of vertical crustal deformation. Quaternary Science Reviews 166: 10–37. https://doi.org/10.1016/j.quascirev.2016.11.011

DiBiase RA, Whipple KX, Heimsath AM, Ouimet WB (2010). Landscape form and millennial erosion rates in the San Gabriel Mountains, CA. Earth and Planetary Science Letters 289 (1–2): 134–144. https://doi.org/10.1016/j.epsl.2009.10.036

Djamour Y, Vernant P, Bayer R, Nankali HR, Ritz JF et al. (2010). GPS and gravity constraints on continental deformation in the Alborz Mountain range, Iran. Geophysical Journal International 183: 1287–1301. https://doi.org/10.1111/j.1365-246X.2010.04811.x

Duvall A, Kirby E, Burbank D (2004). Tectonic and lithologic controls on bedrock channel profiles and processes in coastal California. Journal of Geophysical Research 109: F03002. https://doi.org/10.1029/2003JF000086

Flint JJ (1974). Stream gradient as a function of order, magnitude and discharge. Water Resources Research 10: 969–973. https://doi.org/10.1029/WR010i005p00969

Gardner TW (1983). Experimental study of knickpoint and longitudinal profile evolution in cohesive, homogeneous material. Geol. Geological Society of America Bulletin 94: 664-672. https://doi.org/10.1130/0016-7606(1983)94<664:ESOKAL>2.0.CO;2

Guest B, Axen GJ, Lam PS, Hassanzadeh J (2006). Late Cenozoic shortening in the west-central Alborz Mountains, northern Iran, by combined conjugate strike-slip and thin-skinned deformation. Geosphere 2 (1): 35–52. https://doi.org/10.1130/GES00019.1

Guest B, Guest A, Axen GJ (2007). Late Tertiary tectonic evolution of northern Iran: A case for simple crustal folding. Global and Planetary Change 589 (1-4): 35-53. https://doi.org/10.1016/j.gloplacha.2007.02.014

Haghipour N, Burg JP (2014). Geomorphological analysis of the drainage system on the growing Makran accretionary wedge. Geomorphology 209: 111–132. https:// doi.org/10.1016/j.geomorph.2013.11.030

Hayakawa YS, Oguchi T (2006). DEM-based identification of fluvial knickzones and its application to Japanese Mountain Rivers. Geomorphology 78: 90–106. https://doi. org/10.1016/j.geomorph.2006.01.018

Hayakawa YS, Oguchi T (2009). GIS analysis of fluvial knickzone distribution in Japanese mountain watersheds. Geomorphology 111: 27–37. https://doi.org/ 10.1016/j.geomorph.2007.11.016

Iranian Seismological Center, Institute of Geophysics, University of Tehran (2022). Website www.irsc.ut.ac.ir

Jackson J, Priestley K, Allen M, Berberian M (2002). Active tectonics of the South Caspian Basin. Geophysical Journal International 148 (2): 214 –245. https://doi.org/10.1046/j.1365- 246X.2002.01588.x

Jansen JD, Fabel D, Bishop P, Xu S, Schnabel C et al. (2011). Does decreasing paraglacial sediment supply slow knickpoint retreat? Geology 39: 543-546. https://doi.org/10.1130/G32018.1

Kaveh-Firouz A, Mohammadi A, Görüm T, Sarıkaya MA, Alizadeh H et al. (2023). Main drivers of drainage pattern development in onshore Makran Accretionary Wedge, SE Iran. International Journal of Earth Sciences 112: 539–559. https://doi:10.1007/s00531-022-02270-6

Kirby E, Whipple KX (2001). Quantifying differential rock-uplift rates via stream profile analysis. Geology 29 (5): 415–418. https://doi.org/10.1130/0091-7613(2001)029<0415:QDRURV>2.0.CO;2

Kirby E, Whipple KX, Tang W, Chen Z (2003). Distribution of active rock uplift along the eastern margin of the Tibetan Plateau: inferences from bedrock channel longitudinal profiles. Journal of Geophysical Research 108 (B4): 22-17. https://doi.org/10.1029/ 2001JB000861

Kirby E, Whipple KX (2012). Expression of active tectonics in erosional landscapes. Journal of Structural Geology 44: 54–75. https://doi.org/10.1016/j.jsg.2012.07.009

Koons PO, Upton Ph, Barker AD (2012). The influence of mechanical properties on the link between tectonic and topographic evolution. Geomorphology 137 (1): 168-180. https://doi.org/10.1016/j.geomorph.2010.11.012

Mandal SK, Burg JP, Haghipour N (2017). Geomorphic fluvial markers reveal transient landscape evolution in tectonically quiescent southern Peninsular India. Geological Journal 52 (4): 681-702. https://doi.org/10.1002/gj.2833

Martins AA, Cabral J, Cunha PP, Stokes M, Borges J et al. (2017). Tectonic and lithological controls on fluvial landscape development in central-eastern Portugal: insights from long profile tributary stream analyses. Geomorphology 276: 144–163. https://doi.org/10.1016/j.geomorph.2016.10.012

Madanipour S, Ehlers TA, Yassaghi A, Rezaeian M, Enkelmann E et al. (2013). Synchronous deformation on orogenic plateau margins: insights from the Arabia–Eurasia collision. Tectonophysics 608: 440–451. https://doi.org/10.1016/j.tecto.2013.09.003

Merritts D, Vincent K (1989). Geomorphic response of coastal streams to low, intermediate, and high rates of uplift, Medocino triple junction region, northern California. Geological Society of America Bulletin 101 (11): 1373-1388. https://doi.org/10.1130/0016-7606(1989)101<1373:GROCST>2.3.CO;2

Miller JR (1991). The influence of bedrock geology on knickpoint development and channel-bed degradation along downcutting streams in south-central Indiana. The Journal of Geology 99: 591-605. https://doi.org/10.1086/629519

Molnar P, Anderson RS, Anderson SP (2007). Tectonics, fracturing of rock, and erosion. Journal of Geophysical Research 112: F03014. https://doi.org/10.1029/2005JF000433

Nazari H (2006). Analyse de la tectonique récente et active dans l'Alborz Central et la région de Téhéran: Approche morphotectonique et paléoseismologique. PhD, University of Montpellier, France (in French)Nazari H, Ritz JF (2008). Neotectonics in Central Alborz, special issue. Geosciences 17: 75-92. (hal-00811586)

Nazari H, Ritz JF, Shafei A, Ghassemi A, Salamati R et al. (2009), Morphological and paleoseismological analyses of the Taleghan fault, Alborz, Iran. Geophysical Journal International 178: 1028–1041. https://doi:10.1111/j.1365-246X.2009.04173.x.

Nazari H, Ritz JF, Salamati R, Shahidi A, Habibi H et al. (2010). Distinguishing between fault scarps and shorelines: the question of the nature of the Kahrizak, North Rey and South Rey features in the Tehran plain (Iran). Terra Nova 22 (3): 227-237. https://doi:10.1111/j.1365-3121.2010.00938.x

Nazari H, Ritz JF, Walker RT, Salamati R, Rizza M et al. (2014). Palaeoseismic evidence for a medieval earthquake, and preliminary estimate of late Pleistocene slip-rate, on the Firouzkuh strike-slip fault in the Central Alborz region of Iran. Journal of Asian Earth Sciences 82: 124-135. https://doi.org/10.1016/j.jseaes.2013.12.018

Peri VG, Haghipour N, Christl M, Terrizzano C, Kaveh-Firouz A et al. (2022). Quaternary landscape evolution in the Western Argentine Precordillera constrained by 10Be cosmogenic dating. Geomorphology 396: 107984. https://doi.org/10.1016/j.geomorph.2021.107984

Phillips JD, McCormack S, Duan J, Russo JP, Schumacher AM et al. (2010). Origin and interpretation of knickpoints in the big south Fork river basin, Kentucky Tennessee. Geomorphology 114: 188-198. https://doi.org/10.1016/j.geomorph.2009.06.023

Reneau Sl (2000). Stream incision and terrace development in Frijoles Canyon, Bandelier National Monument, New Mexico, and the influence of lithology and climate. Geomorphology 32(1-2): 171-193. https://doi.org/10.1016/S0169-555X(99)00094-X

Rieben H (1955). The geology of the Teheran Plain. American Journal of Science 253: 617– 639. https://doi.org/10.2475/ajs.253.11.617

Ritz JF, Nazari H, Ghassemi A, Salamati R, Shafei A et al. (2006). Active transtension inside Central Alborz: A new insight of the Northern Iran-Southern Caspian geodynamics. Geology 34: 477–480. https://doi.org/10.1130/G22319.1

Ritz JF, Nazari H, Balescu S, Lamothe M, Salamati R et al. (2012). Paleoearthquakes of the past 30,000 years along the North Tehran Fault (Iran). Journal of Geophysical Research Atmospheres 117: B06305. https://doi.org/10.1029/2012JB009147

Saberi E, Yassaghi A, Djamour Y (2017). Application of geodetic leveling data on recent fault activity in Central Alborz, Iran. Geophysical Journal International 2011: 751–765. https:// doi.org/10.1093/gji/ggx311

Schumm SA, Dumont JF, Holbrook JM (2000). Active tectonics and alluvial rivers. Cambridge University Press, pp.276.

Snyder NP, Whipple KX, Tucker GE, Merritts DJ (2000). Landscape response to tectonic forcing: digital elevation model analysis of stream profiles in the Mendocino triple junction region, northern California. Geological Society of America Bulletin 112: 1250–1263. https://doi.org/10.1130/0016-7606(2000)112<1250:LRTTFD>2.0.CO:2

Solaymani Azad SH, Ritz JF, Abbassi MR (2011). Left-lateral active deformation along the Mosha–North Tehran fault system (Iran): Morphotectonics and paleoseismological investigations. Tectonophysics 497 (1-4): 1-14. https://doi.org/10.1016/j.tecto.2010.09.013

Stock JD, Montgomery DR (1999). Geologic constraints on bedrock river incision using the stream power law. Journal of Geophysical Research 104 (B3): 4983–4993. https://doi.org/10.1029/98JB02139

Stöcklin J (1968). Structural history and tectonics of Iran: a review. American Association of Petroleum Geologists bulletin 52 (7): 1229-1258. https://doi.org/10.1306/5D25C4A5-16C1-11D7-8645000102C1865D

Vernant P, Nilforoushan F, Hatzfeld D, Abbassi MR, Vigny C et al. (2004). Present-day crustal deformation and plate kinematics in Middle East constrained by GPS measurement in Iran and northern Oman. Geophysical Journal International 157: 381–398. https://doi.org/10.1111/j.1365-246X.2004.02222.x

Whipple KX, Tucker GE (1999). Dynamics of the stream-power river incision model: implications for height limits of mountain ranges, landscape response timescales, and research needs. Journal of Geophysical Research 104: 17661–17674. https://doi.org/10.1029/ 1999JB900120

Whipple KX, Wobus C, Crosby B, Kirby E, Sheehan D (2007). New Tools for Quantitative Geomorphology: Extraction and Interpretation of Stream Profiles from Digital Topographic Data. NSF Geomorphology and Land Use Dynamics.

Wei Z, Bi L, Xu Y, He H (2015). Evaluating knickpoint recession along an active fault for paleoseismological analysis: the Huoshan Piedmont, Eastern China. Geomorphology 235: 63–76. https://doi.org/10.1016/j.geomorph.2015.01.013

Wobus C, Whipple KX, Kirby E, Snyder N, Johnson J et al. (2006). Tectonics from topography: procedures, promise, and pitfalls. Tectonics, Climate, and Landscape Evolution 398: 55–74. https://doi.org/10.1130/2006.2398 (04)

Yassaghi A, Madanipour S (2008). Influence of a transverse basement fault on along-strike variations in the geometry of an inverted normal fault: case study of the Mosha fault, central Alborz range, Iran. Journal of Structural Geology 30: 1507–1519. https://doi.org/ 10.1016/j.jsg.2008.08.006

Yildirim C, Schildgen TF, Echtler H, Melnick D, Strecker MR (2011). Late Neogene and active orogenic uplift in the Central Pontides associated with the North Anatolian Fault: Implications for the northern margin of the Central Anatolian Plateau, Turkey. Tectonics 30 (5). https://doi.org/10.1029/2010TC002756

Zanchi A, Berra F, Mattei M et al. (2006) Inversion tectonics in central Alborz, Iran. Journal of Structural Geology 28 (11): 2023-2037. https://doi.org/10.1016/j.jsg.2006.06.020

Zaprowski BJ, Evenson EB, Pazzaglia FJ, Epstein JB (2001). Knickzone propagation in the Black Hills and northern high plains: a different perspective on the late Cenozoic exhumation of the Laramide Rocky Mountains. Geology 29: 547-550. https://doi.org/10.1130/0091-7613(2001)029%3C0547:KPITBH%3E2.0.CO;2

Zhang H, Zhang P, Fan Q (2011). Initiation and recession of the fluvial knickpoints: a case study from the Yalu River-Wangtian'e volcanic region, northeastern China. Science China Earth Sciences 54: 1746-1753. https://doi.org/10.1007/s11430-011-4254-6